Challenges and Recommendations for Enhancing Protection of Onshore Wind Farm Collector Systems

A. J. Alves Júnior, M. J. B. B. Davi, D. C. Jorge, D. Barbosa, M. Oleskovicz, and D. V. Coury

***Abstract*—Wind farms are becoming increasingly significant as renewable energy resources continue to expand, largely due to advancements in Inverter-Based Resources (IBRs). As widely reported in the literature, IBRs directly impact the operation of conventional protection. However, much of this research focuses on protecting transmission lines interconnecting IBRs to the primary grid. Assessments of the challenges and solutions for protection systems operating within wind farm collector networks remain limited in the literature. In this context, this research examines the performance of conventional protection functions within a real-world onshore wind farm by conducting realistic simulations on PSCAD/EMTDC software. In addition to addressing the challenges in the operation of overcurrent and directional overcurrent functions through parametric analyses, this paper contributes to the state-of-the-art by presenting tests on commercial relays. It also outlines recommendations for protecting wind farm collector systems. Aspects such as the most promising protection functions and the best positioning of relays to enhance protection schemes are highlighted.**

***Keywords*—Directional Protection, Inverter-Based Resources, Overcurrent Protection, Protection Systems, Wind Farms.**

I. Introduction

WIND energy has rapidly emerged as a prominent source of clean electricity, driven by its economic benefits and crucial role in supporting the global transition to sustainable energy systems [1]. However, integrating Inverted-Based Resources (IBRs), such as wind farms, solar plants, and energy storage systems, into existing power grids introduces various challenges, including issues related to power quality, protection settings, and system stability [2], [3].

Unlike conventional synchronous machines, IBRs exhibit distinct short-circuit characteristics, including a limited fault current magnitude, lack of inertia, and different fault contributions for each sequence component [4]–[6]. These characteristics and fault-ride-through capabilities can significantly impact conventional protection schemes, potentially compromising the overall protection system.

Thus, most studies on IBR protection systems have mainly focused on grid-side interconnection lines, concentrating on modifications and improvements to existing protection schemes, such as differential, undervoltage, distance, and adaptive overcurrent [7]–[9].

Distance protection is one of the most widely applied functions in transmission lines, and the high penetration of IBR introduces challenges to its correct operation, mainly due to the impact on short-circuit currents, fault detection, and impedance calculations [10]. Therefore, the use of communication technologies, new innovative algorithms, dynamic trip region adjustment, and non-pilot method to accelerate the second zone of distance relays are vital to improve their performance in power systems with IBR [11], [12].

Furthermore, it is essential to highlight that the existing literature includes studies on the impacts of IBR in other transmission line protections, such as line protection by phase comparison [13]; negative sequence-based overcurrent and directional overcurrent functions [14]; line differential function [15], [16]; phase selection functions [17], [18]; among others. However, the studies above focus on analyzing the impact of IBRs on interconnection line protection.

In this context, it should be noted that analyses on the operation of protection schemes within IBRs power plants are scarce in the literature. Only a few studies address this topic, focusing primarily on the configuration of each wind turbine's protection systems. The performance of these generating units under fault conditions is analyzed in [19]. At the same time, the required protection adjustments for the wind farm collection systems, incorporating directional overcurrent elements, are detailed in [20]. Wind farm protection analyses have been carried out in large-scale installations, such as the Al-Zaafarana wind farm in Egypt [21] and the Penonomé wind farm in Panama [22]. However, these studies do not clearly state the challenges of protecting wind farm collector systems as a whole nor provide recommendations for overcoming these challenges.

Despite studies involving the protection of electric power systems with wind turbines, some even relating to real cases [23], [24], a notable gap in the literature is the lack of detailed examination of collector system protection. In many wind farm collector systems, the combined contributions from the grid

The authors would like to thank the Sao Paulo Research Foundation (FAPESP) [#2022/00483-0] and the National Council for Scientific and Technological Development (CNPq) for their financial support. They also gratefully acknowledge the support of the RCGI Research Centre for Greenhouse Gas Innovation, hosted by the University of São Paulo (USP), sponsored by FAPESP São Paulo Research Foundationă[#2020/15230-5], and sponsored by TotalEnergies, and the strategic importance of the support given by ANP (Brazils National Oil, Natural Gas and Biofuels Agency) through the R&DI levy regulation. A. J. Alves Júnior is with the University of São Paulo, São Carlos, Brazil (e-mail of corresponding author: alailtonjunior@usp.br). M. J. B. B. Davi, D. C. Jorge, D. Barbosa, M. Oleskovicz, and D. V. Coury are with the University of São Paulo, São Carlos, Brazil (e-mails: moisesdavi@usp.br; davidcjorge@alumni.usp.br; dbarbosa@ufba.br; olesk@sc.usp.br; coury@sc.usp.br).

Paper submitted to the International Conference on Power Systems Transients (IPST2025) in Guadalajara, Mexico, June 8-12, 2025.

and the IBRs can lead to abnormal fault current profiles–such as significant current magnitude reduction or even reverse faulted power flow–especially under high fault resistance conditions. These atypical behaviors can result in conventional protection schemes failing to detect faults effectively, posing a risk to system stability and reliability.

Thus, recognizing the importance of analysis on this topic, this research investigates the performance of conventional protection functions within a real-world onshore wind farm. By conducting realistic simulations on the PSCAD/EMTDC software, this study aims to evaluate the effectiveness of protections between collector busbars and IBRs. The main contributions of this research to the state-of-the-art can be summarized as follows.

- Parametric analyses are carried out focusing on the operation of overcurrent and directional overcurrent protection functions conventionally embedded in commercial protection devices, aiming to both characterize and prove the challenges that wind farm collector system topologies present to conventional protection operation;
- Tests are conducted on commercial relays to validate the discussions and presented findings;
- Recommendations for protecting wind farm collector systems are presented, highlighting the most effective protection functions and the strategic placement of protection devices that enhance the protection scheme.

II. Test System

To conduct performance analyses of conventional protections, PSCAD software was employed to model an onshore wind power plant with a realistic topology, as shown in Fig. 1. The wind farm in this model consists of Full-Converter generators, with 120 wind turbines with 4.2 MW nominal power, distributed over four collector busbars (C1, C2, C3, and C4). Two four-winding transformers with 280 MVA rated power connect these collector busbars to the main collector bus.

In this study, the modeling of IBRs was based on the Grid-Following (GFL) control strategy [25], [26]. The GFL-IBR synchronizes with the grid voltage and adjusts its internal voltage to ensure that the current commanded by the control loops is achieved. Consequently, the GFL-IBR behaves as a current source. The synchronized angle required for the Park transform is derived from a Phase-Locked Loop (PLL). A conventional three-phase PLL, as described in [27], was adopted and appropriately tuned.

The GFL control structure consists of an inner loop that regulates the output current in the dq reference frame and an outer loop that is responsible for active and reactive power control. Both loops utilize Proportional-Integral (PI) controllers, with gains adjusted using the internal model control approach [28]. The outer loop controllers were designed to operate ten times slower than the inner loop. The converter current limit was defined as 1.1 p.u. The IBR was configured to operate at a unity power factor during steady-state operation. However, when the voltage drops below 0.85 p.u., the control system identifies an abnormal state and commands the converter to inject a positive sequence reactive current [29]. Since the modeled system represents a real wind farm located in Brazil, the operational and fault ride-through requirements are in accordance with the country's grid code [30].

To enable fault analysis within the wind power plant and given that the topologies of the individual collector bus circuits have similar characteristics, only one circuit of collector C2 was selected for detailed analysis and fault simulation. In this circuit, an overhead line is employed, with its impedances specified in Fig. 2. Fault scenarios were simulated at various locations, including at 0%, 50%, and 100% of the entrance collector line, as well as at other points. The remaining circuits of the C2 collector bus and other collectors were modeled using equivalent representations based on the methodology presented in [31].

Besides varying the fault locations, as depicted in Fig. 2, the simulations also considered changing the fault types (AG, AB, ABG, and ABC), fault resistances (0, 5, 10, 15, 20, 30, 40, 50, 75 and 100 Ω) and fault inception angles (0, 45, and 90 degrees). Finally, the wind plant's generation level was varied between 0.1, 0.5, and 1 p.u. of the nominal power.

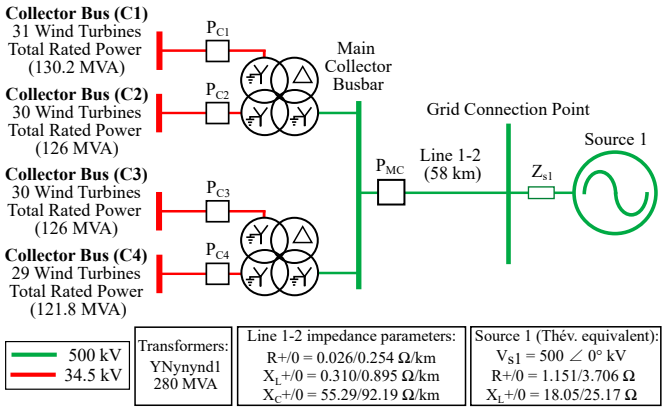

Fig. 1. Test system single-line diagram and parameters.

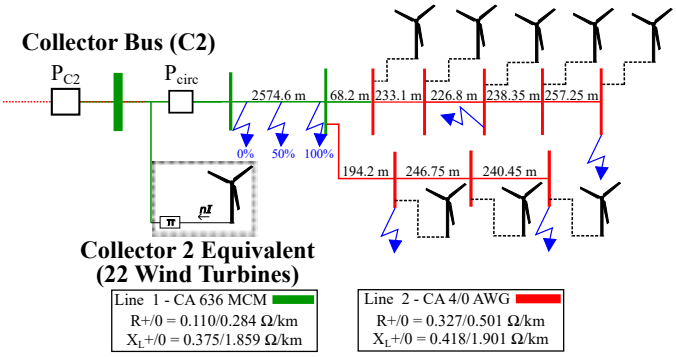

Fig. 2. Single-line diagram with fault points for the C2 collector's detailed circuit.

Therefore, considering all the variations regarding generation level and fault parameters, 2,520 fault scenarios were analyzed. Two measurement levels were considered: measurements on the secondary of the C2 collector bus transformer (P_{C2}) and measurements at the entrance of the detailed collector C2 circuit (P_{circ}). All the assessments

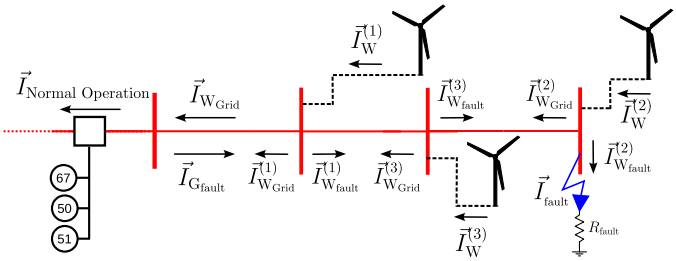

Fig. 3. Fault current flow in an internal fault in a wind farm.

focused on one of the collector circuits (C2). However, all considerations are also valid for other collector circuits in the wind power plant.

III. Technical Background on the Challenges of Wind Farm Collector System Protection

Considering the system topologies described in Section II, the simulation and analysis of electrical faults within the wind farm reveal atypical behaviors in the faulted phase current [32]. The challenges identified in the simulations, and subsequently faced by the protection systems within wind farm collector systems, primarily concern fault detection occurring between the collector and the IBRs.

In traditional radial distribution lines, fault current decreases as fault resistance increases. As resistance increases, the fault becomes less detectable by the system, resulting in a current close to the nominal load flowing through it. This behavior, however, may differ significantly in wind farm collector systems.

To understand the behavior of fault currents in wind farms, it is essential to recognize the distinct characteristics of these systems compared to conventional radial networks. In wind farms, the fault current I_{fault} is conceptually expressed as the sum of contributions from each wind turbine ($I_{W_{\text{fault}}}$) and the primary grid ($I_{G_{\text{fault}}}$), as presented in a simplified form in (1). This expression is intended to capture the overall contribution trend while the detailed nonlinear dynamics and control interactions are comprehensively analyzed through PSCAD/EMTP simulations.

$$I_{\text{fault}} = I_{G_{\text{fault}}} + \sum_{i=0}^{n} I_{W_{\text{fault}}}^{(i)} \tag{1}$$

During an internal fault, as depicted in Fig. 3, each IBR effectively sees the fault as a parallel load to the grid. Its contribution to the fault current, $I_{W_{\text{fault}}}$, can be estimated by (2), while the remaining current, $I_{W_{\text{Grid}}}$, is exported to the primary grid, as shown in (3).

$$I_{W_{\text{fault}}} = I_W \left(\frac{Z_{eq}}{R_f + Z_{eq}} \right) \tag{2}$$

$$I_{W_{\text{Grid}}} = I_W \left(\frac{R_f}{R_f + Z_{eq}} \right) \tag{3}$$

where Z_{eq} is the grid equivalent impedance seen at the faulted position, and I_W is the current supplied by the wind turbine. Additionally, the grid's contribution to the fault, $I_{G_{\text{fault}}}$, can be estimated by (4).

$$I_{G_{\text{fault}}} = \frac{V_G}{R_f + Z_{eq}} \tag{4}$$

Consequently, the current measured at the collector bus, I_{bus}, is the difference between the faulted current provided by the primary grid and the portion of each wind turbine's current that flows to this grid, as described in (5).

$$I_{Bus} = I_{G_{\text{fault}}} - \sum_{i=0}^{n} I_{W_{\text{Grid}}}^{(i)} \tag{5}$$

Therefore, within a wind farm collector bus, the fault current contribution dynamics change due to contributions from the primary grid and IBRs. As fault resistance increases, the current measured at the collector bus decreases more rapidly. This is because the IBRs begin to supply power to the fault and the rest of the system. In scenarios with high fault resistance, this dynamic can even cause a reversal in the direction of the faulted power flow.

This behavior is illustrated in Fig. 4, where a single-phase fault located at the end of the collector line (100% of the line length) was selected from the simulated conditions. Using the measurement point at the collector bus (P_{C2}), this setup allows for a comparison of the fault current magnitude and angle at 10%, 50%, and 100% of IBRs nominal power. The current phasors shown were calculated after 18 post-fault cycles when the transient had stabilized.

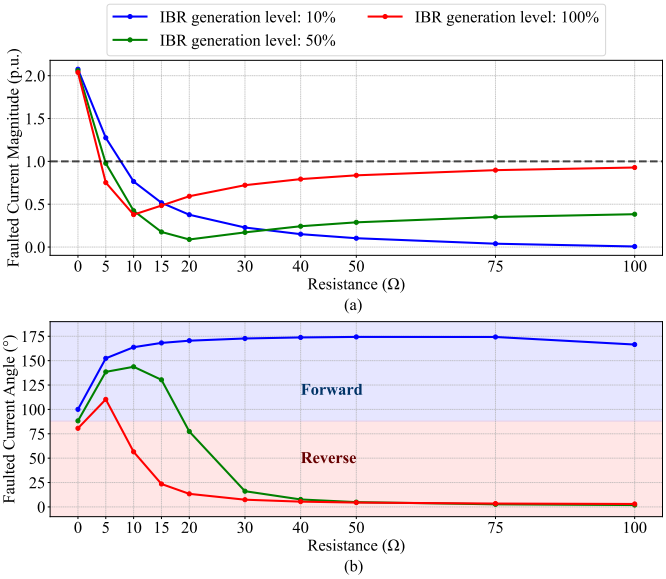

Fig. 4. Fault current magnitude (a) and angle (b) comparison for different IBR penetration level

As shown in 4(a), increasing the penetration of IBR results in a more rapid decline in the magnitude of the fault current as the resistance to the fault increases. Initially, as the fault resistance rises from zero, the fault current decreases until it reaches a minimum threshold. This threshold is reached when the fault current supplied by the grid is balanced by the current injected by the IBR to the grid during the fault; at this balance point, the overall measured current is minimized.

Beyond this point, further increases in fault resistance lead to a shift in the current contributions: the current provided by

the IBRs to the grid begins to exceed the grid's contribution to the fault. This shift causes a reversal in the fault current direction, indicating that, despite the occurrence of a fault within the wind farm, the IBRs are exporting power to the primary grid. This current reversal is clearly depicted in 4(b), where the fault current angle moves into the red zone–defined as angles between 0ř and 90ř–representing reverse power flow. For instance, at 100% IBR penetration, the current reversal is observed when the fault resistance exceeds $10, \Omega$, whereas, at 50% penetration, the reversal occurs at approximately $30, \Omega$. These observations underscore that under certain conditions, the IBRs continue to supply power to the grid, thereby altering the conventional fault current profile.

Moreover, the location at which the fault current is measured plays a critical role in its interpretation. At the collector bus, where multiple circuits feed into the IBRs, additional infeed currents from parallel circuits can lead to a significantly lower measured fault current than that observed within an individual circuit. This effect is illustrated in 5, which shows that, for a 100% generation level of the IBRs, the same fault condition yields a reduced fault current when measured at the collector bus.

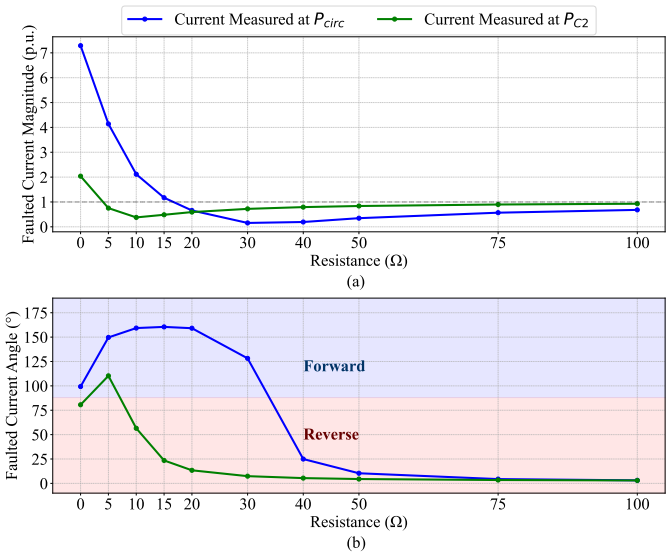

Fig. 5. Fault current comparison for (a) magnitude and (b) angle from different measuring locations

Overall, these findings reveal two key challenges for traditional protection schemes in wind farm collector systems: (i) the marked drop in fault current magnitude due to the balancing contributions of the grid and the IBRs, and (ii) the reversal of current flowevidenced by a shift in the fault current anglethat complicates fault detection by directional protection. These complex behaviors highlight the need for more sophisticated fault detection and protection strategies tailored to systems with high IBR penetration.

IV. Computational Assessment of Conventional Protection Performance

To illustrate the challenges discussed in Section III, this section presents a case study focusing on the conventional protection functions employed at the wind farm collector bus in the simulated test system.

A. Theoretical Background of the Evaluated Protection Functions

The primary protection functions utilized in wind farm collector systems are overcurrent protection (ANSI 50/51) and directional overcurrent protection (ANSI 67). These protection schemes rely on the magnitude and phase angle of the current phasors to operate.

ANSI 50/51 protection operates solely on the current magnitude. This scheme is typically configured with a pickup current, a fixed threshold above the nominal current, beyond which the protection function is activated.

In contrast, the ANSI 67 protection considers the current magnitude and phase angle, allowing it to operate only when the current flows in a specified direction. This directional protection is configured with a pickup current and a phase angle, which together define the criteria for operation.

Given that the collector current is expected to be exported from the wind farm, ANSI 67 protection is particularly well suited for protecting the collector bus, as it can readily detect the current flow inversion, signaling a fault condition.

The operating principle of ANSI 67 protection is based on comparing the measured current with the reference phasors, as described in [33]. This principle is illustrated through (6), (7), and (8), which describe the operating current for the phase, neutral, and negative sequence components, respectively.

$$I_{op_{67P}} = |I_p| \times \cos\left[\angle\underline{I_p} - \left(r + \angle\underline{V_{ref}}\right)\right] \tag{6}$$

$$I_{op_{67N}} = |I_0| \times \cos\left[\angle\underline{I_0} - \left(r + \angle\underline{V_0}\right)\right] \tag{7}$$

$$I_{op_{67Q}} = |I_2| \times \cos\left[\angle\underline{I_2} - \left(r + \angle\underline{V_2}\right)\right] \tag{8}$$

Where p represents the phase index corresponding to phases a, b and c, while V_{ref} refers to the reference voltage, derived from the phase-to-phase voltages V_{bc}, V_{ca} and V_{ba}. Specifically, V_{bc} serves as the reference voltage for phase a, V_{ca} for phase b, and V_{ba} for phase c. Furthermore, $|I_0|$ and $|I_2|$ represent zero and negative currents and $|V_0|$ and $|V_2|$ zero and negative voltages, respectively. In all three equations, the variable r is the relay characteristic angle (RCA), which accounts for the phase shift introduced by the relay settings.

The pickup and trip signal of this protection is determined by comparing the operating current with the predetermined pickup current, as described in (9).

$$\begin{aligned}
\text{Pickup}_{67P} &= \begin{cases} 1 & \text{if } I_{op_{67P}} \geq I_{67P}, \\ 0 & \text{otherwise.} \end{cases} \\
\text{Pickup}_{67N} &= \begin{cases} 1 & \text{if } I_{op_{67N}} \geq I_{67N}, \\ 0 & \text{otherwise.} \end{cases} \\
\text{Pickup}_{67Q} &= \begin{cases} 1 & \text{if } I_{op_{67Q}} \geq I_{67Q}, \\ 0 & \text{otherwise.} \end{cases}
\end{aligned} \tag{9}$$

Table I presents the parameters used to configure the ANSI 67 protection in the simulation and in the commercial device

tested. These values were selected based on the study in [34], adapted to the specific test system used in this research. Since the system analyzed in [34] has different transformer power capacity and wind turbine ratings compared to our setup, the current pickup values were scaled proportionally to reflect the power capacity of our system.

TABLE I
PARAMETERS OF THE ANSI 67 PROTECTION

Function	Pickup Current	Angle (RCA)
ANSI 67P	220 A	30°
ANSI 67N	110 A	10°
ANSI 67Q	110 A	30°

B. Results for Protection Performance Assessments

The performance of the protection functions was evaluated by simulating a wide range of fault scenarios in the test system. The scenarios tested the protection functions under various conditions, including fault types, locations, resistances, and levels of power wind penetration.

The evaluation was carried out at two distinct measuring points in the collector bus: the entrance of the collector bus (P_{C2}) and the entrance of the detailed circuit (P_{circ}). Due to the extensive number of simulated fault points, the analyses presented below focus on the most distant fault point from the measuring point, representing the worst scenario.

Figs. 6, 7, 8, and 9 illustrate the behavior of the magnitude and angle of the fault current as functions of resistance for various types of faults and levels of penetration of the wind at the collector bus. The regions labeled Forward and Reverse in the angle graphics indicate the respective directions of the current in phase A, using the voltage in phase A as a reference. The region where the phasor angle is between $[-90, 90]$, corresponding to the first and fourth quadrants, is classified as Reverse. Conversely, the region where the angle is outside this range, corresponding to the second and third quadrants, is considered Forward.

In the figures, the dashed lines represent the results recorded in the collector bus, while the solid lines correspond to the results at the entrance of the detailed circuit. The performance of the protection system is indicated by the colors of the markers, as explained in Table II. Specifically, blue markers denote cases where at least one variant of ANSI 67 detected the fault; black markers indicate detection only by 67N and 67Q; and red markers signify that the fault was not detected.

TABLE II
LEGEND FOR PROTECTION PERFORMANCE ASSESSMENT RESULTS

Marker	Description
●	Fault detected by the ANSI 67 protection function. (67P or 67N or 67Q)
●	Fault detected by the neutral or negative protection, but not by the phase protection. (67N OR 67Q)
●	Fault not detected.

In Fig. 6, which depicts single-phase faults to the ground, three distinct stages of behavior are observed. The current magnitude initially exceeds the nominal level with low fault resistance. As resistance increases, the current magnitude decreases and enters a second stage, remaining below the nominal level. During this phase, the fault angle does not reverse, which means that the fault might still be detected. In the third stage, the fault angle reverses as the resistance increases and the current magnitude increases again. This reversal, as well as the subsequent increase in current magnitude, complicates fault detection with conventional ANSI 67 protection functions.

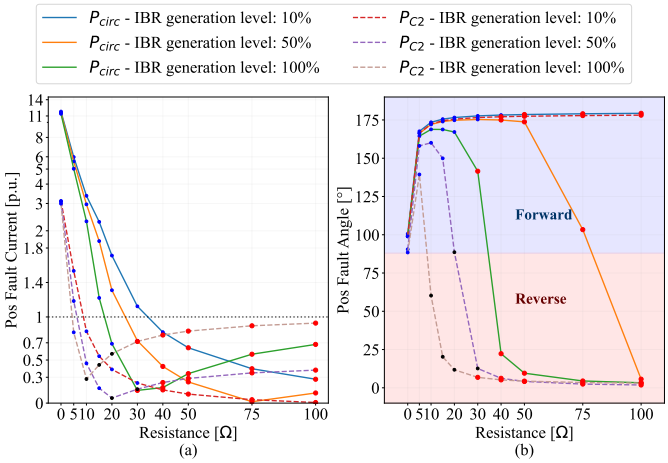

Fig. 6. Phase-to-Ground Fault: Fault current (a) magnitude and (b) angle vs. resistance across wind penetration levels at the Collector Bus.

Figs. 7 and 8 present the behavior of phase-phase-ground and phase-phase faults, respectively. These types of faults exhibit the same behavior regarding the resistance of the fault to phase-ground faults. The current magnitude initially decreases with increasing fault resistance but begins to rise again when the fault angle reverses.

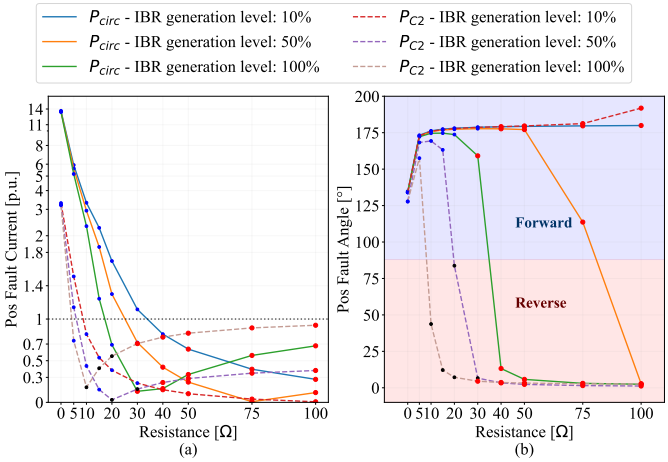

Fig. 7. Phase-to-Phase-to-Ground Fault: Fault current (a) magnitude and (b) angle vs. resistance across wind penetration levels at the Collector Bus.

In contrast, Fig. 9 illustrates three-phase fault behavior, where the same pattern is noticed, but the current magnitude remains relatively high even with increased resistance. The increased current magnitude typically enhances the ability to detect faults more effectively than other fault types. However, it is important to note that only the phase ANSI 67P protection function is applicable to this fault type.

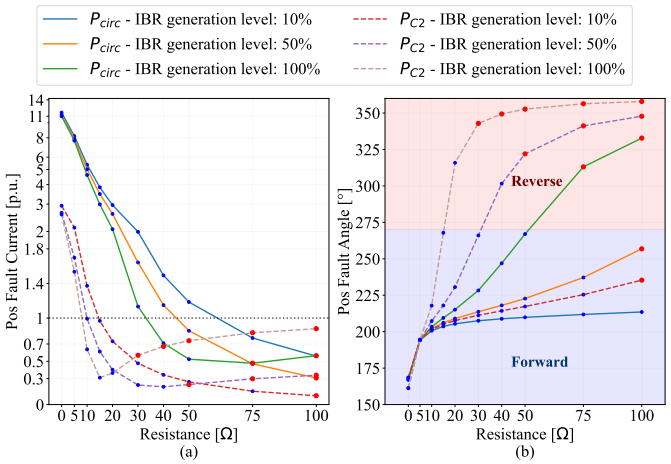

Fig. 8. Phase-to-Phase Fault: Fault current (a) magnitude and (b) angle vs. resistance across wind penetration levels at the Collector Bus.

The performance of the ANSI 67 protection functions varies significantly across different scenarios. The ANSI 67P function does not detect faults in the collector bus when the fault resistance is high, as seen in Figs. 7 and 8 for resistances of 15Ω and 20Ω. In contrast, the ANSI 67N and ANSI 67Q functions show better detection capabilities in those scenarios. However, there are instances where none of the protection functions successfully detect the fault, indicating limitations in ANSI 67 efficacy.

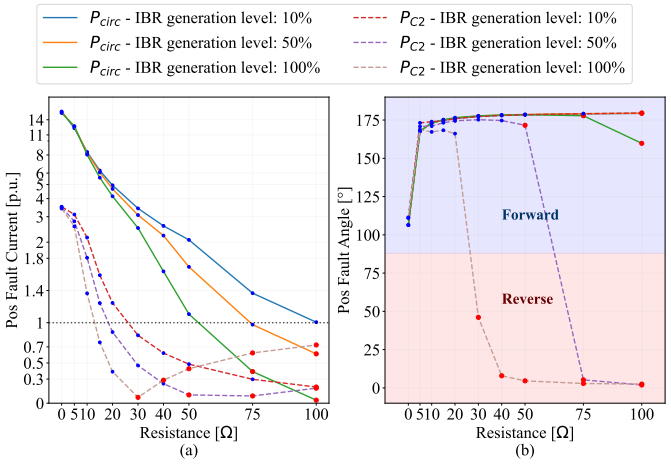

Fig. 9. Three-Phase Fault: Fault current (a) magnitude and (b) angle vs. resistance across wind penetration levels at the Collector Bus.

As shown in the figures, higher wind power penetration levels further exacerbate the challenge of detecting faults. As the proportion of IBR's power increases, more current is injected into the grid during the fault, which causes the lower magnitude in the fault current or when the IBR's contribution to the grid is higher to the grid contributions to the fault, occurs the reversal in the fault current angle, imposibilitantion the fault detection by the ANSI 67 element.

In the collector bus, the most distant measuring point from the fault often represents the worst scenario. Thus, the increased influence from other parallel circuits contributes to the more significant decrease in current magnitude at this point, making fault detection difficult for even low fault resistances by the relay.

In conclusion, traditional ANSI 50/51 and ANSI 67 protection functions encounter significant limitations when detecting faults on the collector bus. The ANSI 50/51 function, solely reliant on the current magnitude, cannot be effectively parameterized for currents below the nominal level. This limitation severely hinders its applicability in scenarios with low fault currents, as presented in the above analyses.

In contrast, while the ANSI 67 function offers more versatility due to its dependence on the current direction, it struggles to detect faults at higher resistances, particularly up to 30Ω. This issue is exacerbated by higher IBR penetration levels, which can cause a reversal of fault power flow, as IBRs inject current into the grid during a fault.

Fault types such as phase-ground and phase-phase-ground present particular challenges due to their lower current magnitudes, which impede fault detection. This is primarily caused by the delta-wye transformer connection between the wind turbines and the overhead lines, where IBRs only inject current into the grid and do not contribute directly to the fault current.

Consequently, three-phase and phase-phase faults, which typically have higher fault current magnitudes, tend to be more easily detected. This is because IBRs contribute current to both the fault and the grid, depending on the fault resistance. As a result, the current measured at the collector bus or the circuit entrance is less influenced by IBRs infeed during faults.

Furthermore, while our analysis focuses on a specific wind farm configuration, the fundamental challenges we identified are not limited to this setup. The interaction between short-circuit levels at the collector bus and the substantial power injection from wind turbines is a widespread issue in wind farm collector systems. We expect similar challenges to occur across various configurations, including larger onshore installations and offshore wind farms with different topologies.

These findings underscore the necessity for enhancing conventional protection mechanisms to improve their reliability and effectiveness, especially in systems with significant wind power penetration.

V. Performance Tests with Commercial Protection Devices

This section conducts a comprehensive evaluation of commercial protection devices employed for fault detection in a simulated wind farm environment. The analysis specifically examines the efficacy of directional overcurrent protection systems under two divergent fault scenarios: one characterized by low fault resistance, facilitating fault detection, and the other by high fault resistance, which presents substantial challenges to the protection relay.

Thus, to validate the performance of commercial protection devices, the waveforms of these two scenarios were replicated using the test set represented in Fig. 10, and the commercial IED was configured with the same settings used in the computational simulations.

Figs. 11 and 12 show the waveforms recorded by commercial protection devices and digital channels of the

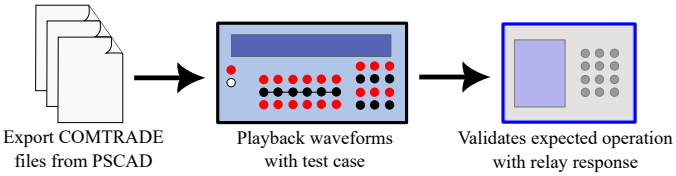

Fig. 10. Testing set.

ANSI 67P, ANSI 67N, and ANSI 67Q functions, considering the low and high fault resistance scenarios, respectively. It is essential to note that high-resistance faults undermine the performance of protection functions, potentially leading to the misoperation of the commercial IED.

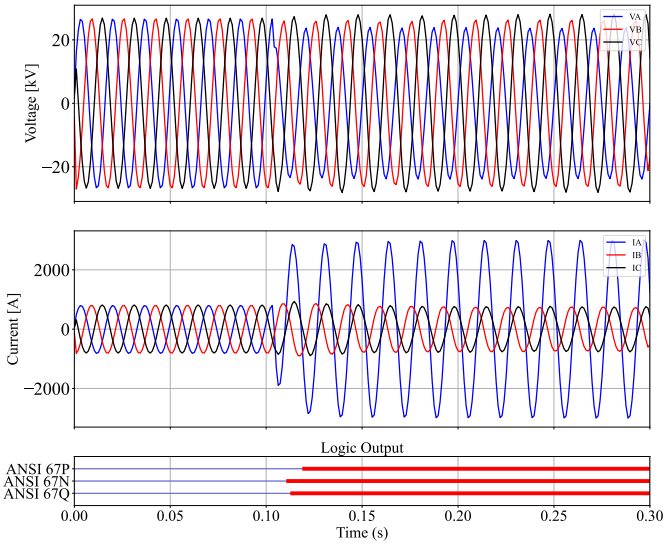

Fig. 11. Performance of the IED in a single-phase fault with 5Ω resistance.

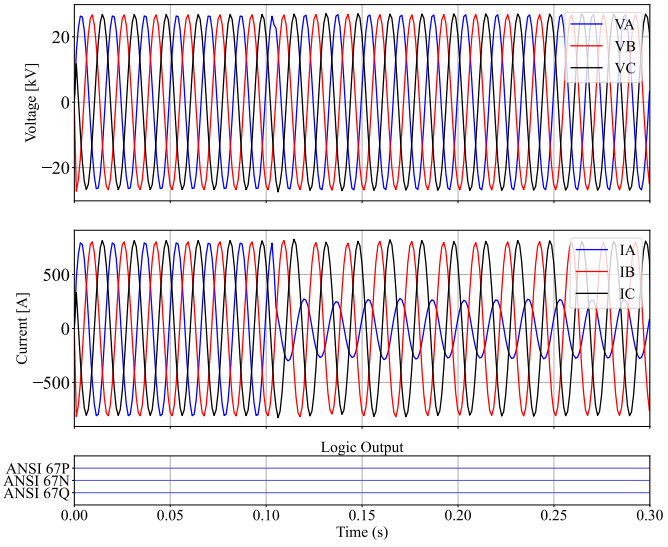

Fig. 12. Performance of the IED in a single-phase fault with 50Ω resistance.

VI. Overview on Recommendations for Wind Farm Collector Systems Protection

Based on the analysis of protection performance under various faults in the simulation scenarios, some recommendations can be made to enhance the effectiveness of protection systems in these environments.

Firstly, it is evident that the ANSI 50/51 protection functions must be better suited for wind farm collector systems. The current magnitude in these systems often falls below the nominal current, which significantly impairs the effectiveness of ANSI 50/51 for fault detection. This limitation arises because ANSI 50/51 relies on threshold settings that may not be appropriately calibrated for the lower current levels typically observed in such systems.

In contrast, the ANSI 67 protection functions offer a more robust performance. The analysis demonstrates that ANSI 67 provides improved fault detection capabilities, mainly when implemented with phase (ANSI 67P) and sequence components (ANSI 67N for neutral and ANSI 67Q for negative sequences). The results indicate that ANSI 67N and ANSI 67Q can detect faults missed by ANSI 67P alone. This improved detection is attributed to the unbalanced three-phase currents and voltages during fault conditions, which can be more effectively identified using sequence components.

Moreover, the proximity of the measuring point to the fault plays a critical role in the performance of the protection system. The closer the measuring point is to the fault, the more effectively the protection system can operate. This occurs because a measuring point closer to the fault minimizes the influence of other turbines in the measured current.

In summary, the findings suggest that while ANSI 50/51 may not be adequate for protecting wind farm collector systems, ANSI 67 provides a more effective solution with its phase, neutral, and negative sequence components. Additionally, optimizing the placement of measuring points closer to fault locations can further improve the performance of protection systems. Implementing these recommendations can significantly enhance fault detection and reliability in wind farm collector systems.

VII. Conclusions

This study has comprehensively analyzed the challenges of protecting wind farm collector systems, particularly regarding the unique behavior of fault currents influenced by IBR. Through extensive simulations utilizing PSCAD/EMTDC and practical testing of commercial relays, it has been demonstrated that conventional protection functions, specifically ANSI 50/51 and ANSI 67, struggle to effectively address the distinct characteristics of fault currents found in wind farms. Thus, careful parametrization of the protection settings and determination of the relay location within the collector system are essential to ensure reliable fault detection, including the infeed of currents from multiple circuits.

The results indicate that these conventional protection functions could be limited by the lower magnitudes and altered dynamics of fault currents compared to those in traditional power systems. Therefore, adopting ANSI 67N and ANSI 67Q protection functions and adjusting relay settings to accommodate the reduced fault current levels typically observed in wind farm environments help avoid protection misoperation. However, as outlined in Section IV and demonstrated in Section V, There are fault scenarios

in which these conventional functions are not effectively sensitized, underscoring the issues illustrated in this paper and necessitating further investigation in future work.

In conclusion, this research addresses a gap in the existing literature regarding protection challenges within wind farm collector systems. The practical insights and recommendations offer valuable guidance for enhancing the design and operation of protection schemes in these systems, although further protection schemes are needed to effectively protect the collector system.

REFERENCES

[1] M. H. Saeed, W. Fangzong, B. A. Kalwar, and S. Iqbal, "A review on microgrids challenges & perspectives," *IEEE Access*, vol. 9, pp. 166 502–166 517, 2021.

[2] M. Eissa (SIEEE), "Protection techniques with renewable resources and smart gridsa survey," *Renewable and Sustainable Energy Reviews*, vol. 52, pp. 1645–1667, 2015.

[3] M. Nagpal and C. Henville, "Impact of power-electronic sources on transmission line ground fault protection," *IEEE Transactions on Power Delivery*, vol. 33, no. 1, pp. 62–70, 2018.

[4] N. Nimpitiwan, G. T. Heydt, R. Ayyanar, and S. Suryanarayanan, "Fault current contribution from synchronous machine and inverter based distributed generators," *IEEE Transactions on Power Delivery*, vol. 22, no. 1, pp. 634–641, 2007.

[5] A. Hooshyar and R. Iravani, "Microgrid protection," *Proceedings of the IEEE*, vol. 105, no. 7, pp. 1332–1353, 2017.

[6] M. J. Reno, S. Brahma, A. Bidram, and M. E. Ropp, "Influence of inverter-based resources on microgrid protection: Part 1: Microgrids in radial distribution systems," *IEEE Power and Energy Magazine*, vol. 19, no. 3, pp. 36–46, 2021.

[7] A. A. Memon and K. Kauhaniemi, "A critical review of ac microgrid protection issues and available solutions," *Electric Power Systems Research*, vol. 129, pp. 23–31, 2015.

[8] S. A. Hosseini, H. A. Abyaneh, S. H. H. Sadeghi, F. Razavi, and A. Nasiri, "An overview of microgrid protection methods and the factors involved," *Renewable and Sustainable Energy Reviews*, vol. 64, pp. 174–186, 2016.

[9] S. Beheshtaein, R. Cuzner, M. Savaghebi, and J. M. Guerrero, "Review on microgrids protection," *IET Generation, Transmission & Distribution*, vol. 13, no. 6, pp. 743–759, 2019.

[10] M. O. Donovan, N. Barry, and J. Connell, "Distance protection of transmission lines connected to inverter-based resources," in *58th International Universities Power Engineering Conf.*, 2023, pp. 1–6.

[11] Y. Xie, Y. Liu, D. Lu, B. Wang, Y. Xu, and Y. Jia, "Distance protection with dynamic trip region for lines terminated by inverter based resources," in *2022 IEEE PES Innovative Smart Grid Technologies - Asia (ISGT Asia)*, 2022, pp. 615–619.

[12] M. M. Mobashsher, A. A. Abdoos, S. M. Hosseini, S. M. Hashemi, and M. Sanaye-Pasand, "An accelerated distance protection scheme for the lines connected to inverter-based resources," *IEEE Systems Journal*, vol. 17, no. 4, pp. 6272–6281, 2023.

[13] A. Haddadi, I. Kocar, J. Mahseredjian, U. Karaagac, and E. Farantatos, "Performance of phase comparison line protection under inverter-based resources and impact of the german grid code," in *2020 IEEE Power Energy Society General Meeting (PESGM)*, 2020, pp. 1–5.

[14] A. Haddadi, M. Zhao, I. Kocar, U. Karaagac, K. W. Chan, and E. Farantatos, "Impact of inverter-based resources on negative sequence quantities-based protection elements," *IEEE Transactions on Power Delivery*, vol. 36, no. 1, pp. 289–298, 2021.

[15] R. Chowdhury, R. McDaniel, and N. Fischer, "Distance elements for line protection applications near unconventional sources," *Schweitzer Engineering Laboratories, Inc.*, 2021.

[16] N. George, O. Naidu, and A. K. Pradhan, "Differential protection for lines connected to inverter-based resources: Problems and solution," in *2022 22nd National Power Systems Conf.*, 2022, pp. 419–424.

[17] A. Hooshyar, E. F. El-Saadany, and M. Sanaye-Pasand, "Fault type classification in microgrids including photovoltaic dgs," *IEEE Trans. on Smart Grid*, vol. 7, no. 5, pp. 2218–2229, 2016.

[18] M. A. Azzouz and A. Hooshyar, "Dual current control of inverter-interfaced renewable energy sources for precise phase selection," *IEEE Transactions on Smart Grid*, vol. 10, no. 5, pp. 5092–5102, 2019.

[19] B. Bak-Jensen, T. A. Kawady, and M. H. Abdel-Rahman, "Coordination between fault-ride-through capability and overcurrent protection of dfig generatorsfor wind farms," in *Proceedings of the 5th Nordic Wind Power Conference*. Technical University of Denmark (DTU), 2009.

[20] D. Jones and K. Bennett, "Wind farm collector protection using directional overcurrent elements," in *PES T&D 2012*, 2012, pp. 1–8.

[21] T. A. Kawady, N. M. Mansour, and A. Taalab, "Wind farm protection systems: state of the art and challenges," *Distributed Generation*, pp. 265–288, 2010.

[22] D. Vila, E. Alcázar, J. Juárez, P. Loza, and H. J. Altuve, "Protection system for a wind generation plant in panama: Challenges and solutions," in *2016 69th Annual Conference for Protective Relay Engineers (CPRE)*. IEEE, 2016, pp. 1–15.

[23] R. Yan, N.-A. Masood, T. Kumar Saha, F. Bai, and H. Gu, "The anatomy of the 2016 south australia blackout: A catastrophic event in a high renewable network," *IEEE Transactions on Power Systems*, vol. 33, no. 5, pp. 5374–5388, 2018.

[24] A. S. Sujo P George, "Malfunction of differential relays in wind farms," *International Journal of Advanced Electrical and Electronics Engineering (IJAEEE)*, vol. 3, pp. 27–31, 2014.

[25] O. Tremblay, R. Gagnon, and M. Fecteau, "Real-time simulation of a fully detailed type-iv wind turbine," in *Proceedings of the IPST*, vol. 13, 2013, pp. 18–20.

[26] N. Miller, J. Sanchez-Gasca, W. Price, and R. Delmerico, "Dynamic modeling of ge 1.5 and 3.6 mw wind turbine-generators for stability simulations," in *2003 IEEE Power Engineering Society General Meeting*, vol. 3, 2003, pp. 1977–1983 Vol. 3.

[27] S.-K. Chung, "A phase tracking system for three phase utility interface inverters," *IEEE Transactions on Power Electronics*, vol. 15, no. 3, pp. 431–438, may 2000.

[28] L. Harnefors and H.-P. Nee, "Model-based current control of AC machines using the internal model control method," *IEEE Transactions on Industry Applications*, vol. 34, no. 1, pp. 133–141, 1998.

[29] S. D. Tavakoli, E. Prieto-Araujo, O. Gomis-Bellmunt, and S. Galceran-Arellano, "Fault ride-through control based on voltage prioritization for grid-forming converters," *IET Renewable Power Generation*, jan 2023.

[30] National Electric System Operator (ONS), "Submodule 2.10 Minimum technical requirements for connection to transmission facilities," Grid Procedures, version 2023.1, May 2023, [Online]. Available: https://www.ons.org.br/. [In Portuguese].

[31] E. Muljadi, S. Pasupulati, A. Ellis, and D. Kosterov, "Method of equivalencing for a large wind power plant with multiple turbine representation," in *2008 IEEE Power and Energy Society General Meeting - Conversion and Delivery of Electrical Energy in the 21st Century*, 2008, pp. 1–9.

[32] M. J. B. B. Davi, M. Oleskovicz, and F. V. Lopes, "An integrated fault detection, classification, and region identification methodology applied to onshore wind farm collector systems," *IEEE Access*, pp. 1–1, 2024.

[33] J. K. N. Stanley H. Horowitz, Arun G. Phadke, *Power System Relaying, 4th Edition*, 4th ed. John Wiley & Sons, 2014.

[34] P. S. Relaying and W. G. C. Control Committee, System Protection Subcommittee C, "Protection of wind electric plants - technical report pes-tr87," 5 2021, p. 75.